buildings

MDPI

Article

Stress Concentration Factors of CHS-to-CFRHS Y-Joints Under Axial Tension Loading

Yisheng Fu [1] and Kuan Diao [2,3,*]

[1] School of Highway, Chang'an University, Xi'an 710064, China; 2020221070@chd.edu.cn
[2] School of Mechanical Science and Engineering, Huazhong University of Science and Technology, Wuhan 430074, China
[3] Guangxi Special Equipment Inspection and Research Institute, Nanning 530299, China
* Correspondence: dk_hust@163.com

Abstract: A CHS-to-CFRHS Y-joint that consists of a circular hollow section (CHS) brace and a concrete-filled rectangular hollow section (CFRHS) chord by welding has a simple and smooth weld profile that saves time and cost for the fabrication of CHS-to-CFRHS Y-joints and leads to a superior fatigue performance, compared with other welded tubular joints. This investigation presented an analysis of the stress concentration factors (SCFs) of CHS-to-CFRHS Y-joints subjected to axial tension loading of the brace. First, a finite element (FE) modelling method, which was validated with the experimental results cited in the reference, was utilised to establish the FE models of CHS-to-CFRHS Y-joints. Then, a parametric analysis was conducted to investigate the influences of the significant non-dimensional geometric parameters on the SCFs of CHS-to-CFRHS Y-joints. It is found that the intersection angle of the brace and chord has an important influence on the magnitudes of the SCF values. An increase in the intersection angle of the brace and chord will increase the values of the SCFs at the 60° location and saddle. The values of the SCFs at the 60° location and saddle reach the maximum value when the intersection angle of the brace and chord reaches 90°. Furthermore, on the basis of the large database of the SCF results, empirical design equations were established to calculate the SCFs at the crown toe, 60° location and saddle via multiple regression analysis. A safety factor was applied to the empirical design equations to ensure safe and reliable results of SCF calculations for the fatigue design of CHS-to-CFRHS Y-joints in a composite truss structure. Ultimately, a comparative analysis of SCFs was conducted with the FE models of welded tubular joints with rectangular hollow section (RHS) chords and CFRHS chords. The results reveal that infilling concrete in the chord leads to a reduction in SCFs along the weld profile of more than 11% on average, and the peak SCF decreases by more than 15%.

Keywords: concrete-filled steel tube chord; CHS-to-CFRHS Y-joint; stress concentration factor; empirical design equations; hot spot stress

check for updates

Academic Editors: Zhe Xing, Yukai Zhong and Ke Jiang

Received: 17 December 2024
Revised: 17 January 2025
Accepted: 18 January 2025
Published: 22 January 2025

Citation: Fu, Y.; Diao, K. Stress Concentration Factors of CHS-to-CFRHS Y-Joints Under Axial Tension Loading. *Buildings* **2025**, *15*, 331. https://doi.org/10.3390/buildings15030331

Copyright: © 2025 by the authors. Licensee MDPI, Basel, Switzerland. This article is an open access article distributed under the terms and conditions of the Creative Commons Attribution (CC BY) license (https://creativecommons.org/licenses/by/4.0/).

1. Introduction

Composite truss structures connected by welded tubular joints with concrete-filled steel tube (CFST) chords are emerging engineering structures that have been increasingly used in engineering projects, such as large spatial structure buildings, truss arch bridges, truss girder bridges, transmission towers, foundation structures of wind turbines and other engineering structures, because of their excellent mechanical properties [1,2]. Numerous studies have indicated that infilling concrete in the chord of a welded tubular joint can improve the bearing capacity, fatigue behaviour and fire endurance over those of its empty

counterpart [3–5]. Previous investigations have focused primarily on welded tubular joints with hollow section chords, such as welded tubular joints with circular hollow section (CHS) braces and CHS chords (CHS-to-CHS joints) (Figure 1a), welded tubular joints with rectangular hollow section (RHS) braces and RHS chords (RHS-to-RHS joints) (Figure 1b) and welded tubular joints with CHS braces and RHS chords (CHS-to-RHS joints). On the basis of the studies on CHS-to-CHS joints, RHS-to-RHS joints and CHS-to-RHS joints, numerous investigation results, such as design parameters, construction measures and empirical design equations, have been adopted in related design standards [6,7]. However, studies on welded tubular joints with CFST chords, such as welded tubular joints with CHS braces and concrete-filled circular hollow section (CFCHS) chords (CHS-to-CFCHS joints), welded tubular joints with RHS braces and concrete-filled rectangular hollow section (CFRHS) chords (RHS-to-CFRHS joints) and welded tubular joints with CHS braces and CFRHS chords (CHS-to-CFRHS joints) (Figure 1c), are relatively limited. To date, numerous investigations on welded tubular joints with CFST chords have been carried out in recent years, and many significant results have been obtained in studies on bearing capacity [8–15], stiffness [16] and fatigue behaviour [17–21]; however, investigations on welded tubular joints with CFST chords are still incomplete and need improvement.

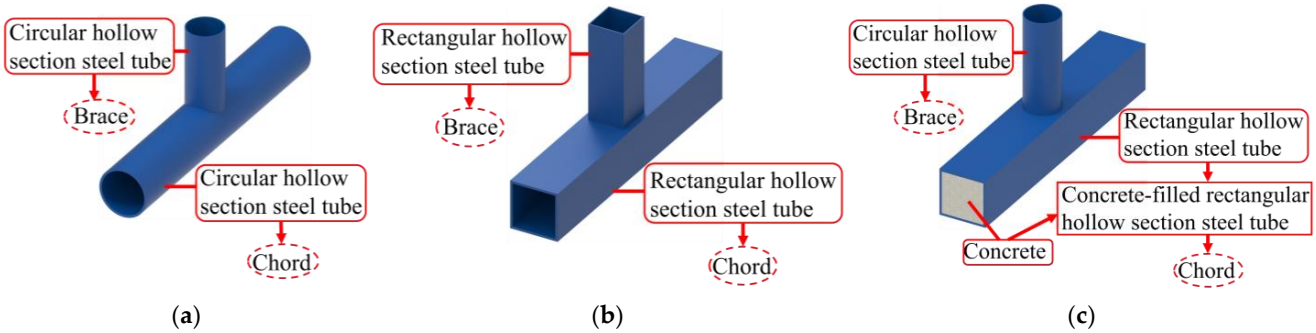


Figure 1. Types of steel tubular joints and composite tubular joints: (**a**) CHS-to-CHS joint; (**b**) RHS-to-RHS joint; and (**c**) CHS-to-CFRHS joint.

As truss structures connected by welded tubular joints are subjected to long-term cyclic loads such as wind and vehicle loads, these welded tubular joints easily suffer from fatigue failure because there are high-stress concentrations near the weld [22]. Consequently, fatigue research is crucial for ensuring the reliable fatigue performance of welded tubular joints. Some investigations have shown that infilling concrete in the hollow section chord can reduce the stress concentrations of welded tubular joints by suppressing the wall deflection of the rectangular section chord and the ovalisation of the circular section chord [23]. Many investigations have considered the influence of infilling concrete in the chord on the stress concentration factor (SCF), which is the ratio of the hot spot stress (HSS) to the nominal stress; this factor is assessed with the HSS method, which is widely employed in fatigue research. Jiang et al. [23,24] investigated SCFs for RHS-to-CFRHS X-joints under axial loading and for RHS-to-CFRHS T-joints subjected to various loading conditions, and the results demonstrated that the SCFs in welded tubular joints were reduced by more than 10% by infilling concrete in the chord. Mashiri et al. [25–29] conducted numerous investigations on RHS-to-CFRHS T-joints and CHS-to-CFCHS T-joints under various loading conditions. Their research demonstrated that the peak SCF of T-joints decreased drastically when concrete was infilled into the chord, and the equations utilised to calculate the SCFs of welded tubular joints with hollow section chords were not appropriate for welded tubular joints with CFST chords. Similar conclusions were drawn by Chen et al. [30], Zheng et al. [31] and Zhao et al. [32].

Previous fatigue investigations on welded tubular joints with CFST chords have focused mainly on CHS-to-CFCHS joints and RHS-to-CFRHS joints, and few investigations have been conducted on CHS-to-CFRHS joints, which have many advantages. Compared with that of CHS-to-CFCHS joints, CHS-to-CFRHS joints have a simpler weld profile, which can reduce the time and cost of fabricating welded tubular joints [33–35]. Compared with RHS-to-CFRHS joints, which have identical geometric parameters and loading conditions, CHS-to-CFRHS joints have lower SCFs and superior fatigue performance [33–35]. Compared with CHS-to-RHS joints, which are traditional structural forms among welded tubular joints in truss structures, CHS-to-CFRHS joints have longer fatigue lives and superior structural performance [36,37]. In conclusion, owing to the superior structural performance of CHS-to-CFRHS joints, research on CHS-to-CFRHS joints is meaningful. In the study of CHS-to-CFRHS joints, one of the key aspects is fatigue research, as welded tubular joints easily suffer from fatigue failure. Tong et al. [38,39] investigated CHS-to-CFRHS T-joints subjected to various loading conditions via finite element analysis and the experimental method and derived empirical design equations to calculate the SCFs of CHS-to-CFRHS T-joints. Their investigations revealed that the maximum SCF value in CHS-to-CFRHS T-joints subjected to axial tension loading of the brace is approximately 67% of that of CHS-to-RHS T-joints on average. However, their investigations of CHS-to-CFRHS joints have focused mainly on T-joint, which is only a special type of Y-joints. Research on the influence of the intersection angle of brace and chord on the stress concentrations of CHS-to-CFRHS joints is lacking. Additionally, the design equations proposed in their investigations for SCF calculations are only applicable for CHS-to-CFRHS T-joints and are not suitable for CHS-to-CFRHS Y-joints, which are commonly used in truss structures. As a result, the present paper studies the effects of the intersection angle of brace and chord on the SCFs of CHS-to-CFRHS Y-joints and establishes the general design equations, which can be used to calculate the SCFs, of CHS-to-CFRHS Y-joints with various intersection angle of brace and chord.

In this work, the stress concentrations of CHS-to-CFRHS Y-joints subjected to axial tension loading of the brace are investigated. First, a finite element (FE) modelling method, which is validated with the experimental results cited in the reference, is used to establish 320 FE models of CHS-to-CFRHS Y-joints. Then, a parametric analysis is carried out to determine the influences of the non-dimensional geometric parameters on the SCFs of CHS-to-CFRHS Y-joints. On the basis of the large database of the SCF results, a multiple regression analysis method is used to derive the empirical design equations for SCF calculations at the crown toe, 60° location and saddle of CHS-to-CFRHS Y-joints. Ultimately, a comparative analysis of the SCFs between the CHS-to-CFRHS Y-joints and the CHS-to-RHS Y-joints is carried out to determine the influence of concrete infilled into chords on the SCFs along the weld profile and the peak SCF of welded tubular joints.

2. FE Model and Verification

2.1. FE Model

As shown in Figure 2, a CHS-to-CFRHS Y-joint consists of a CHS brace and a CFRHS chord. The stress concentrations of CHS-to-CFRHS Y-joints, which were subjected to unit axial tension loading of the brace, were studied via the numerical simulation method in this research, and the FE models of the CHS-to-CFRHS Y-joints shown in Figure 3 were established in the FE software ABAQUS 6.14. To avoid the influence of end constraints, for the FE models of the CHS-to-CFRHS Y-joints, the ratio of length to width was established as six for the chord and the brace [40]. The geometric parameters of the FE models of the CHS-to-CFRHS Y-joints were as follows: the chord members had the same width of 400 mm, with a variable wall thickness ranging from 12.5 mm to 32 mm. The brace members

had widths ranging from 80 mm to 320 mm, with wall thicknesses varying from 3.125 mm to 32 mm.

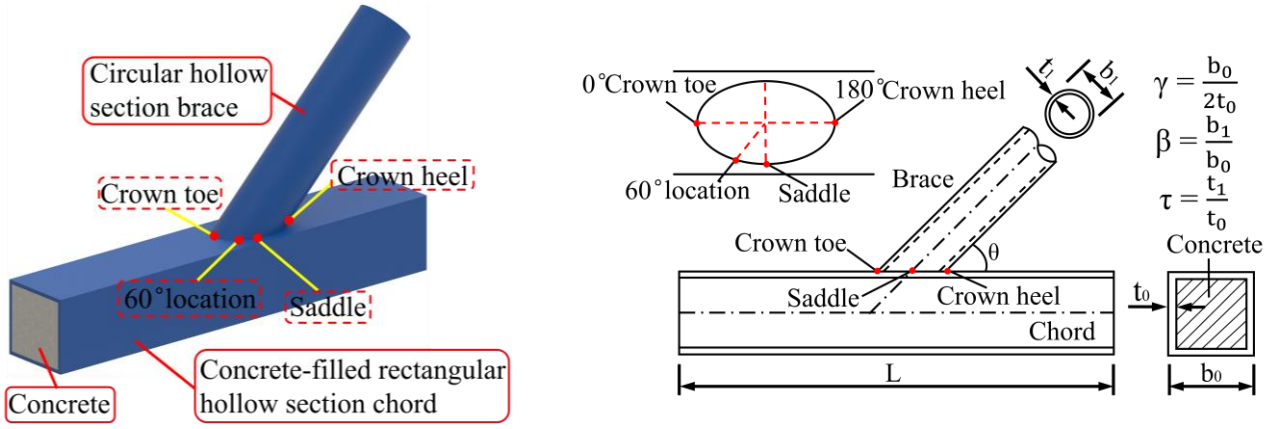


Figure 2. Schematic of the CHS-to-CFRHS Y-joint: (**a**) three-dimensional model of the CHS-to-CFRHS Y-joint; (**b**) geometric parameters of the CHS-to-CFRHS Y-joint.

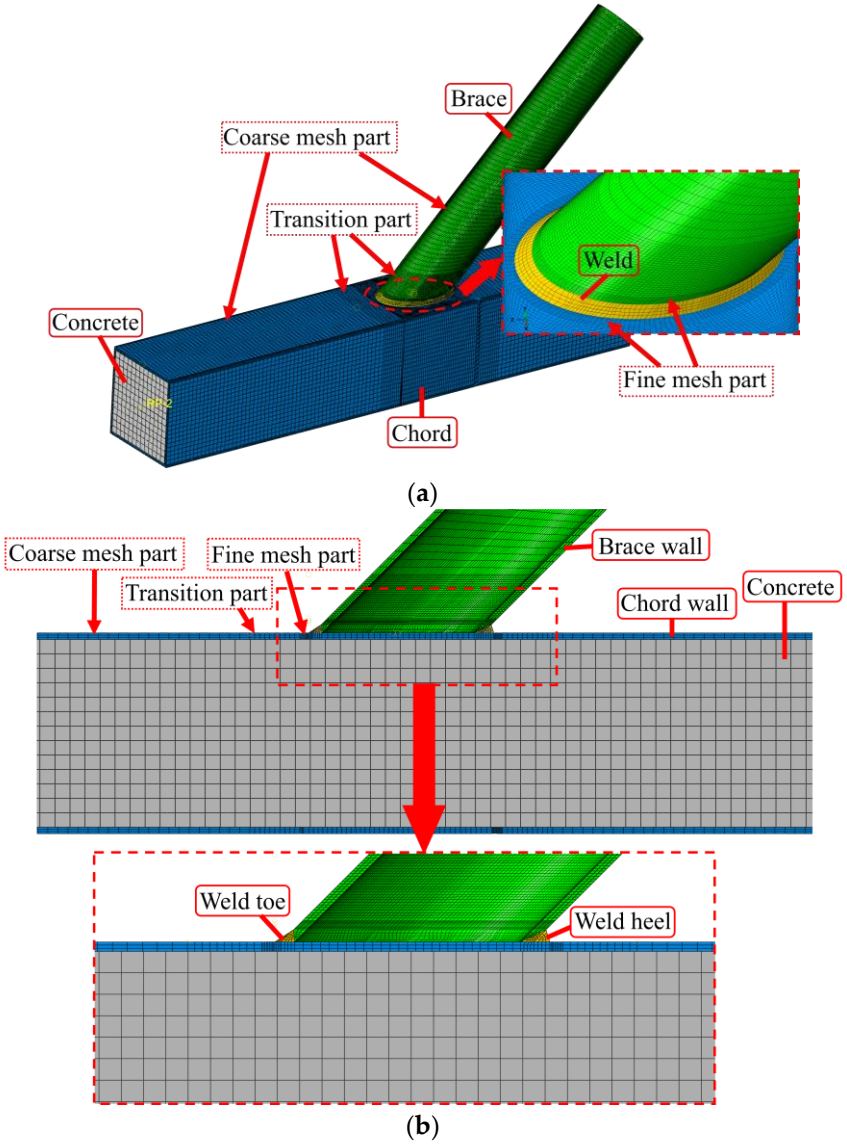
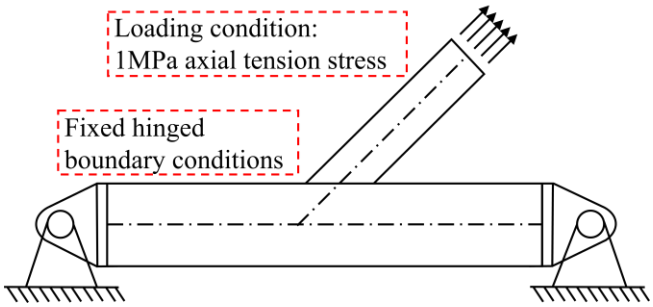


Figure 3. *Cont*.



(**c**)

Figure 3. FE model of the CHS-to-CFRHS Y-joint: (**a**) the entire FE model; (**b**) the central cross-section of the FE model; (**c**) the loading and boundary conditions of the FE model.

The Young's modulus (*E*s) of the steel tube was set to *E*s = 206 GPa; the Poisson's ratio (ν_s) of the steel tube was set to ν_s = 0.3 [41]. The weld metal was set to have material properties identical to those of steel tubes. The Young's modulus of the infilled concrete was assumed to be 34,500 MPa; the Poisson's ratio of the infilled concrete was assumed to be 0.2 [42]. Twenty-node solid quadratic brick elements with reduced integration (C3D20R) were adopted for all the FE models of the CHS-to-CFRHS Y-joints. A refined mesh was utilised in the FE model to obtain SCFs at the hot spot locations around the weld. To reduce the computing time, the mesh was gradually coarsened at locations far from the weld. Fixed hinged boundary conditions were applied at both ends of the chord, as shown in Figure 3c. The free end of the brace was set to the unit axial tension loading condition, ensuring an equivalence relation between the values of the HSS and the SCF.

Setting an appropriate mesh size is important for ensuring the computational efficiency and accuracy of the results. The meshes used in the FE models of the CHS-to-CFRHS Y-joints include fine mesh parts, coarse mesh parts, and transition parts, as shown in Figure 3. The wall thickness mesh on both the chord and the brace of the FE models was divided into three layers [35,39]. The different mesh densities between the outer surface of the concrete infilled into the chord and the inner surface of the chord have little influence on the SCFs in the FE models of the CHS-to-CFRHS Y-joints [23]. Therefore, to reduce the computing time, a coarse mesh was utilised for the infilled concrete.

2.2. Weld Details

The geometric dimensions of the intersecting weld, which is a full penetration weld, comply with the regulations of the American Welding Society (AWS) standard [43], as shown in Figure 3b. The weld profile at the junction of the brace–chord intersection, the detailed parameters of which are presented in Table 1, was adopted as specified in the AWS standard. The weld thickness and weld length are represented by t_w and L, respectively, and the dihedral angle between the brace and chord is denoted by Φ, as illustrated in Figure 4.

Table 1. Details of the weld profile according to the AWS specification.

Parameter	Detail A Ψ = 180–135°	Detail B Ψ = 150–50°	Detail C Ψ = 75–30°	Detail D Ψ = 40–15°
End preparation (ω)				
max.		90°	Needed to obtain required Φ	
min.		10° or 45° for Ψ > 105°	10°	

Table 1. *Cont.*

Parameter	Detail A Ψ = 180–135°	Detail B Ψ = 150–50°	Detail C Ψ = 75–30°	Detail D Ψ = 40–15°
Joint included angle (Φ)				
max.	90°	60° for Ψ ≤ 105°	40°; If more use Detail B	
min.	45°	37–1/2°; If less use Detail C	1/2 Ψ	
Completed weld				
t_w	$\geq t_b$	$\geq t_b$ for Ψ > 90° $\geq t_b/\sin \Psi$ for Ψ < 90°	$\geq t_b/\sin \Psi$ but need not exceed 1.75 t_b	$\geq 2t_b$
L	$\geq t_b/\sin \Psi$ but need not exceed 1.75 t_b		Weld may be built up to meet this	

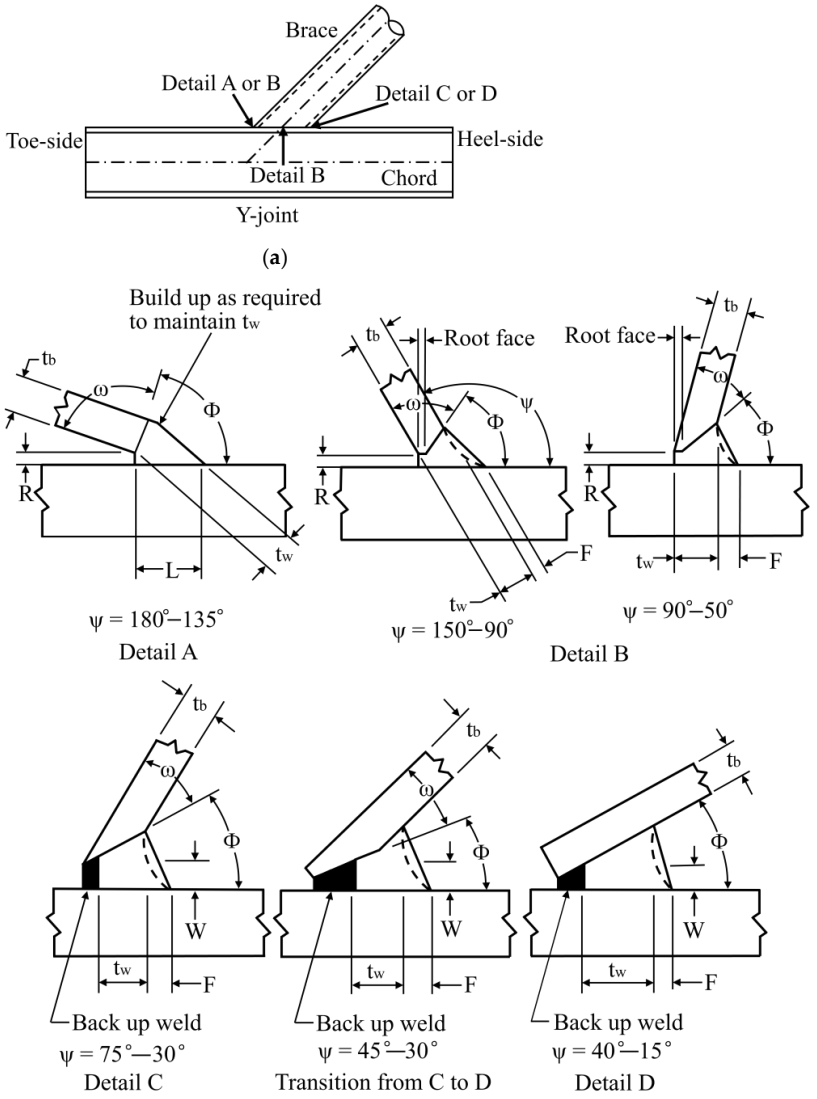


Figure 4. Details of the weld profile in the AWS specification: (**a**) locations of the welding details; (**b**) welding details.

2.3. Steel–Concrete Interface of the CFST Chord of the CHS-to-CFRHS Y-Joint

In the CFST chord of the CHS-to-CFRHS Y-joint, as the adhesion between the outer surface of the infilled concrete and the inner surface of the steel tube is very small, the interface between the steel surface and the concrete surface should separate under interfacial tension in the normal direction in the FE analysis. In the FE models of the CHS-to-CFRHS Y-joints, the contact relationship of the CFST chord includes a tangential friction contact that is defined by the Coulomb friction stress–slip relationship and a normal contact that is defined as a "hard contact" between the steel surface and the concrete surface. Previous studies have shown that a friction coefficient with a value between 0.2 and 0.6 can be adopted in FE analysis [39]. Other studies have also shown that the friction coefficient has little effect on SCFs [44]. Consequently, the friction coefficient was set to 0.35 in the FE models of the CHS-to-CFRHS Y-joints in this research [39].

2.4. Extracting SCFs from the FE Models

The HSS method is widely utilised for assessing the fatigue of welded tubular joints via SCFs and is supported by the International Institute of Welding (IIW) [45], the International Committee for Research and Technical Support for Hollow Section Structures (CIDECT) [46], the American Petroleum Institute (API) [47], the AWS [43] and Det Norske Veritas (DNV) [48]. The SCF values of the CHS-to-CFRHS joints were determined via the HSS method in this research. For CHS-to-CFRHS joints under axial tension loading in the brace, previous research has demonstrated that the SCF distribution in the brace is significantly nonlinear, but the nonlinearity of the SCF distribution in the chord is not obvious [39]. In this research, quadratic extrapolation was used to obtain the HSS for CHS-to-CFRHS Y-joints at the locations close to the weld. The Lagrange quadratic interpolation method was employed to obtain the extrapolation equation, as shown in Equation (1):

$$\sigma_{\mathrm{HSS}} = \frac{t_2 \cdot t_3 \cdot \sigma_1}{(t_1 - t_2) \cdot (t_1 - t_3)} + \frac{t_1 \cdot t_3 \cdot \sigma_2}{(t_2 - t_1) \cdot (t_2 - t_3)} + \frac{t_1 \cdot t_2 \cdot \sigma_3}{(t_3 - t_1) \cdot (t_3 - t_2)} \quad (1)$$

where σ_{i} and t_{j} (i, j = 1, 2, 3) are the stresses of the extrapolation points and the distances from the extrapolation points to the weld, respectively. Following the International Institute of Welding (IIW), three extrapolation points are shown in Figure 5a. With reference to Xiao et al. [1] and Zhao et al. [49], three points are arranged at distances t_1 = 0.4 t, t_2 = 0.9 t and t_3 = 1.4 t away from the weld, as shown in Figure 5b. The HSS can be derived as shown in Equation (2) [49]:

$$\sigma_{\mathrm{HSS}} = 2.52 \cdot \sigma_{0.4t} - 2.24 \cdot \sigma_{0.9t} + 0.72 \cdot \sigma_{1.4t} \quad (2)$$

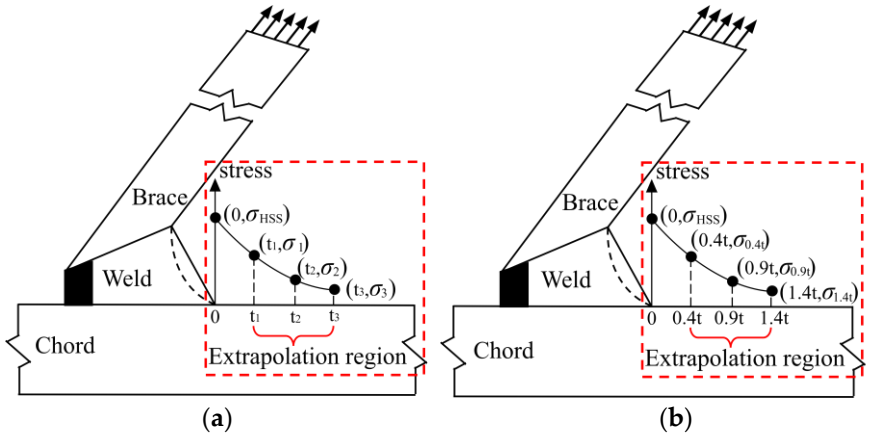


Figure 5. Extrapolation methods for determining the HSS: (**a**) general case; (**b**) special case.

2.5. Verification of the FE Analysis Method

As welded tubular T-joint is a particular type of welded tubular Y-joint, the FE analysis method can be validated with the experimental results of the CHS-to-CFRHS T-joints in Tong et al. [39]. Eight FE models of the CHS-to-CFRHS T-joints, which were subjected to axial tension loading of the brace, with geometric parameters similar to those of the test samples in Tong et al. [39] and weld details designed to meet AWS [43] specifications, were established to verify the correctness of the FE analysis method, as shown in Figure 6. The experimental and calculated SCF values at the key hot spot locations are compared, as shown in Figure 7. Tong et al. [39] obtained the strain concentration factor (SNCF) from experimental results. The SNCF values were converted to SCF values according to the ratio of SCF to SNCF (1.1 on the chord side and 1.2 on the brace side) [39,46]. For specimen T8, the width of the brace was close to the width of the chord, so stress extrapolation was difficult to apply to obtain the HSS in the chord. Consequently, specimen T8 was excluded from the comparative analysis between the FE results and the experimental results of the CHS-to-CFRHS T-joints. The majority of the FE results of the SCF values were consistent with the experimental results. As shown in Table 2, the mean values of the SCF_{FE}-to-SCF_{Text} ratios at key hot spot locations are between 1.04 and 1.13, and the coefficients of variation (COVs) at key hot spot locations are less than 0.16. These results demonstrate the accuracy and reliability of the FE analysis method. A few of the numerical simulation results exhibited significant deviations from the corresponding experimental results. The geometry parameters of the weld profile in the FE models differed from the actual weld profile of the sample, resulting in this deviation.

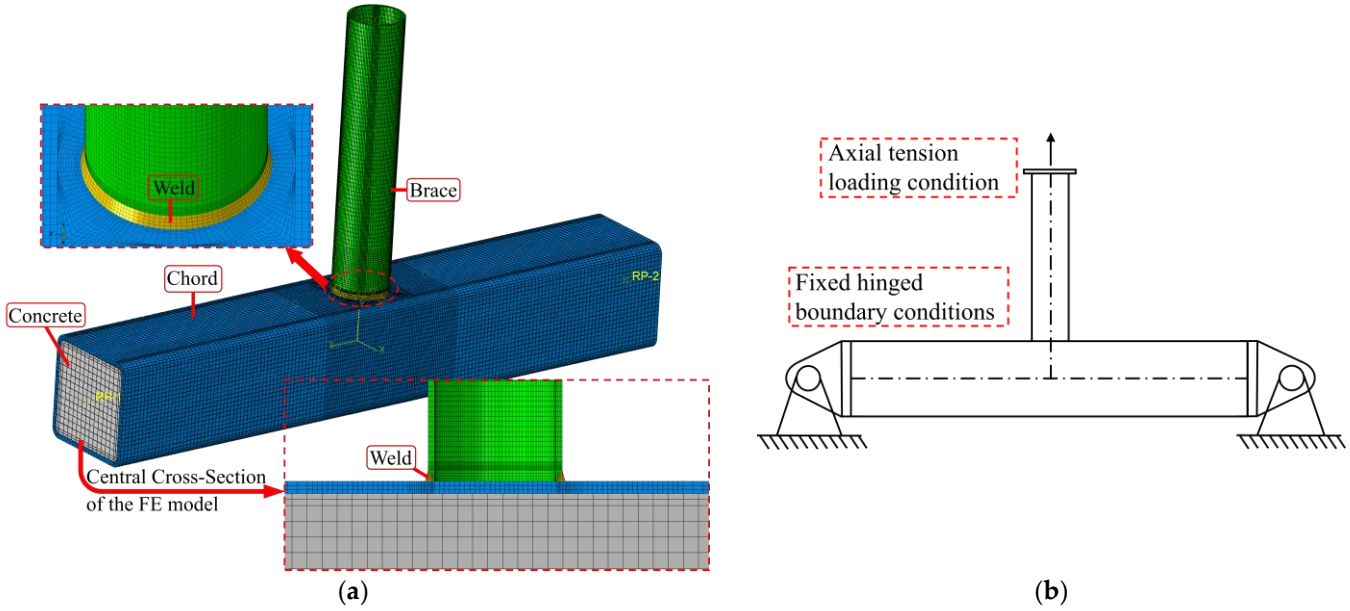


Figure 6. FE model of the text CHS-to-CFRHS T-joint: (**a**) the FE model; (**b**) the loading and boundary conditions of the FE model.

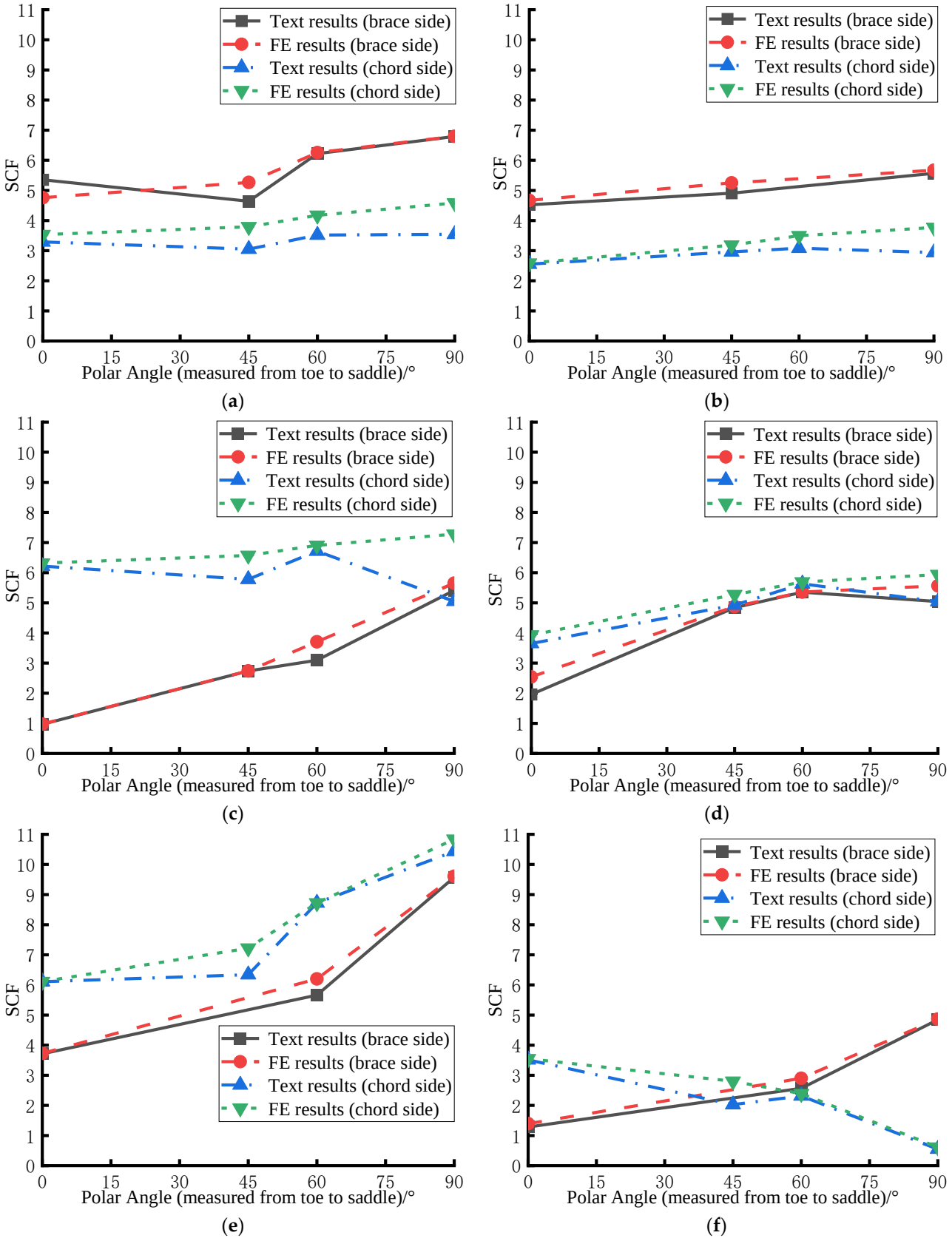
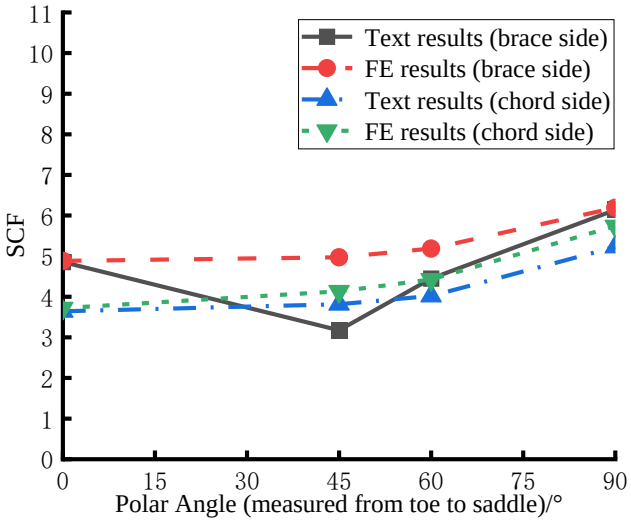


Figure 7. *Cont*.



(**g**)

Figure 7. Comparison of the FE results and the experimental results of the CHS-to-CFRHS T-joints: (**a**) specimen T1; (**b**) specimen T2; (**c**) specimen T3; (**d**) specimen T4; (**e**) specimen T5; (**f**) specimen T6; (**g**) specimen T7.

Table 2. Comparative analysis of the FE results and the experimental results.

SCF_{FE}/SCF_{Text}	Specimen T1	Specimen T2	Specimen T3	Specimen T4	Specimen T5	Specimen T6	Specimen T7
Mean	1.10	1.09	1.11	1.09	1.04	1.11	1.13
COVs	0.12	0.09	0.13	0.09	0.05	0.12	0.16

3. SCF Distribution of CHS-to-CFRHS Y-Joints

To determine the key hot spot locations in the CHS-to-CFRHS Y-joints under axial tension loading in the brace, a comprehensive investigation of the SCF distribution of CHS-to-CFRHS Y-joint was carried out by utilising the single variable method and the parametric analysis method. Previous research has shown that the non-dimensional geometric parameters determined by the standard of CIDECT Design Guide No. 8 [46] have the main influence on SCFs. Consequently, the key hot spot locations in the CHS-to-CFRHS Y-joint can be determined by investigating the variation in the SCF distribution for the CHS-to-CFRHS Y-joint under different single non-dimensional geometric parameter changes. In the CIDECT Design Guide No. 8 [46], the non-dimensional geometric parameters of the SCFs of the welded tubular joints that are intended for the RHS joints and CHS joints but also apply to the CHS-to-CFRHS joints are as follows: the ratio of the width of the brace to the width of the chord ($\beta = b_1/b_0$), the ratio of the width of the chord to the wall thickness of the chord ($2\gamma = b_0/t_0$), the ratio of the wall thickness of the brace to the wall thickness of the chord ($\tau = t_1/t_0$) and the intersection angle of brace and chord (θ), as shown in Figure 2b. A total of 320 FE models of the CHS-to-CFRHS joints were established with the non-dimensional geometric parameters β = 0.2, 0.4, 0.6, and 0.8; γ = 6.25, 10, 12.5 and 16; τ = 0.25, 0.5, 0.75 and 1; and θ = 30°, 45°, 60°, 75° and 90° to study the influence of the non-dimensional geometric parameters on the SCF distribution along the weld path, as shown in Figure 8.

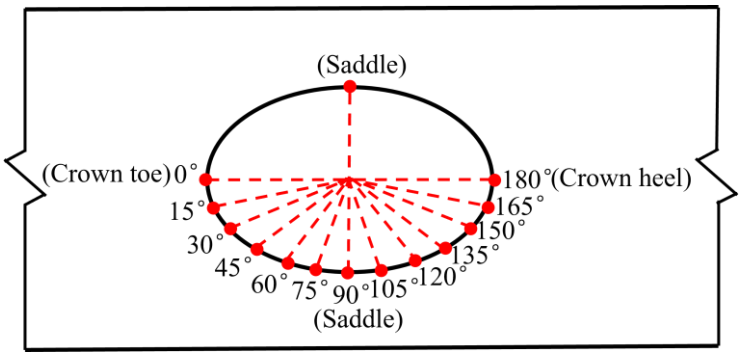


Figure 8. Path of the SCF distribution along the weld profile.

3.1. Influence of β on the SCF Distribution

The influence of β on the SCF distribution of CHS-to-CFRHS Y-joints with identical non-dimensional geometric parameters of γ = 12.5, τ = 0.5 and θ = 45° was investigated by setting different parameters β = 0.2, 0.4, 0.6 and 0.8, as illustrated in Figure 9. When the value of β is between 0.4 and 0.6, the SCFs on both the chord and the brace side reach the maximum values for the given non-dimensional geometric parameters γ, τ and θ. On the brace side, the SCF values generally reach the maximum values at the saddle, whereas on the chord side, the SCF values reach the maximum values at the crown toe or 60° location.

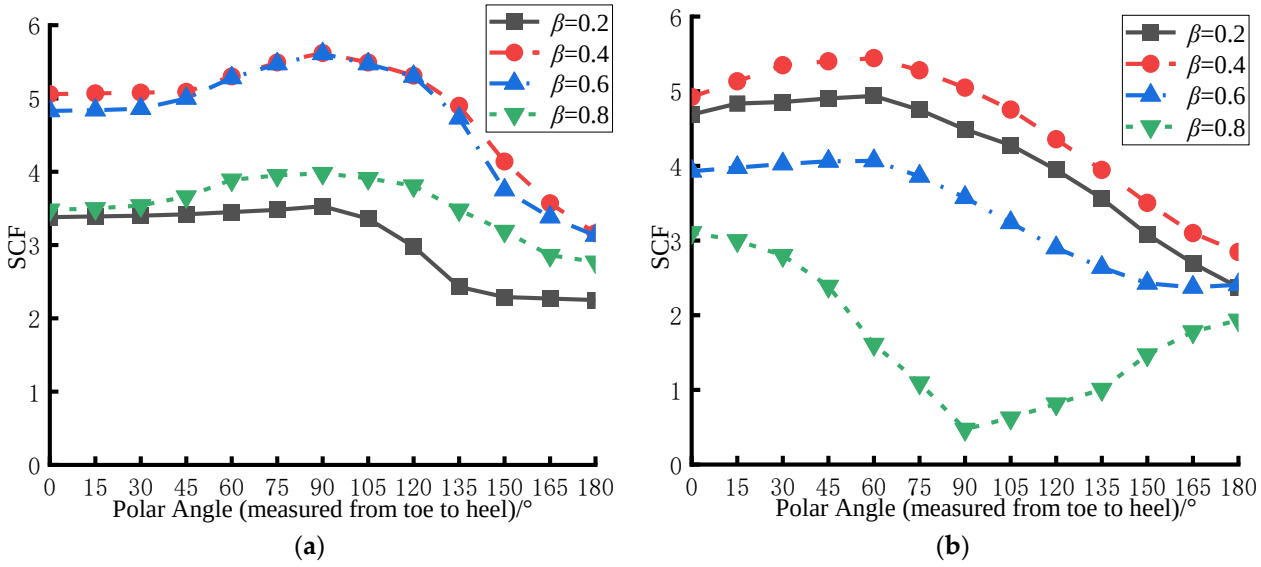


Figure 9. Influence of β on the SCF distribution: (**a**) brace side; (**b**) chord side.

3.2. Influence of γ on the SCF Distribution

The influence of γ on the SCF distribution of CHS-to-CFRHS Y-joints with identical non-dimensional geometric parameters of β = 0.4, τ = 0.75 and θ = 45° was investigated by setting different parameters γ = 6.25, 10, 12.5 and 16, as illustrated in Figure 10. The SCFs on both the chord and the brace side exhibit a similar trend: the SCFs increase at all locations along the weld path with increasing γ. On the brace side, the SCF values generally reach the maximum values at the saddle, whereas on the chord side, the SCF values reach the maximum values at the crown toe or 60° location.

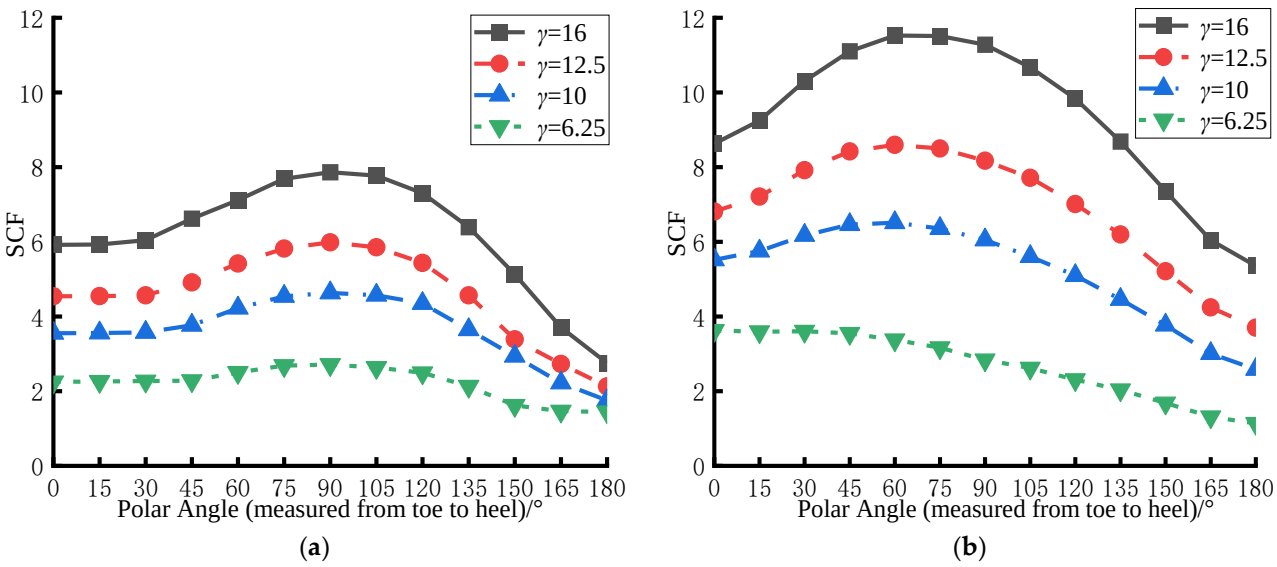


Figure 10. Influence of γ on the SCF distribution: (**a**) brace side; (**b**) chord side.

3.3. Influence of τ on the SCF Distribution

The influence of τ on the SCF distribution of CHS-to-CFRHS Y-joints with identical non-dimensional geometric parameters of $\beta = 0.6$, $\gamma = 10$ and $\theta = 45°$ was investigated by setting different parameters $\tau = 0.25$, 0.5, 0.75 and 1, as illustrated in Figure 11. On the chord side, the SCFs at all locations along the weld path increase as the value of τ increases, but the SCFs on the brace side do not exhibit a clear regularity. The maximum SCF values on the brace side generally occur at the saddle for most cases, whereas on the chord side, the SCF values may reach the maximum values at the crown toe or 60° location.

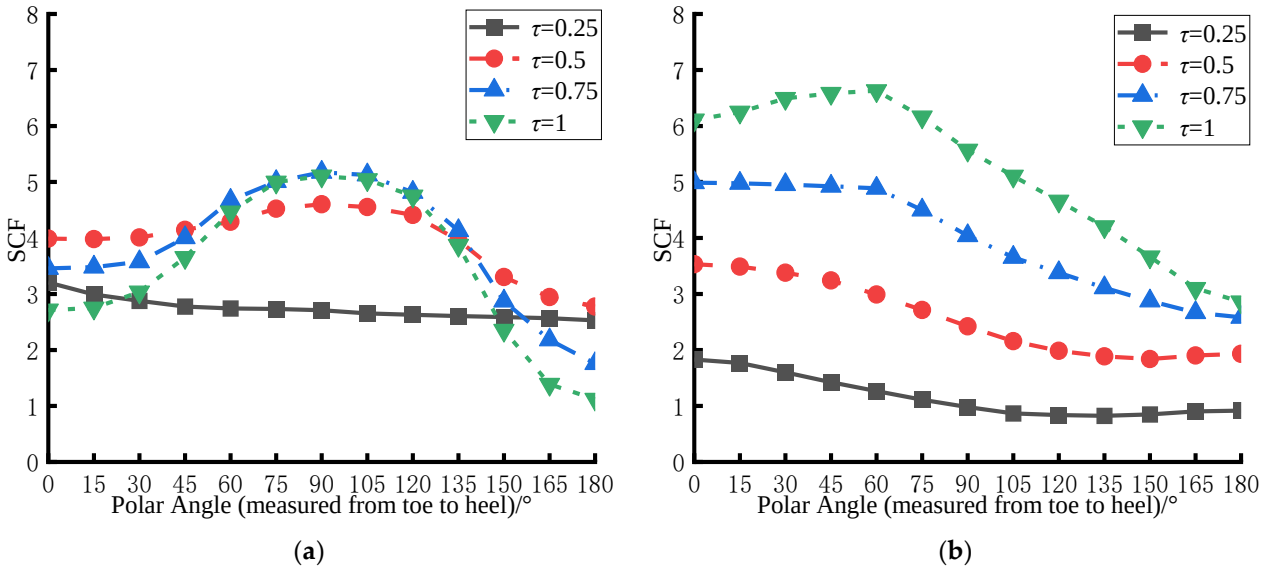


Figure 11. Influence of τ on the SCF distribution: (**a**) brace side; (**b**) chord side.

3.4. Influence of θ on the SCF Distribution

The influence of θ on the SCF distribution of CHS-to-CFRHS Y-joints with identical non-dimensional geometric parameters of $\beta = 0.6$, $\gamma = 12.5$ and $\tau = 0.75$ was investigated by setting different parameters $\theta = 30$, 45, 60, 75 and 90, as illustrated in Figure 12. The maximum SCF values increase as the value of θ increases on both the chord and the brace side. The maximum SCF values on the brace side occur at the saddle, whereas on the

chord side, the SCF values may reach the maximum values at the crown toe, 60° location or saddle.

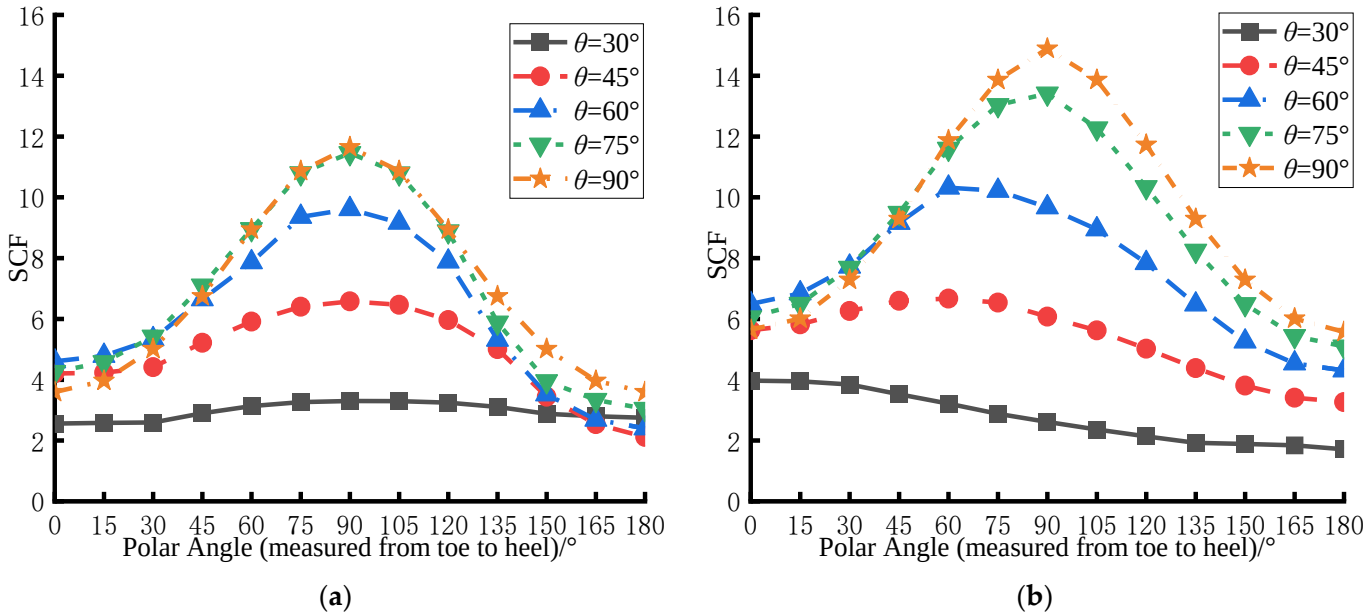


Figure 12. Influence of θ on the SCF distribution: (**a**) brace side; (**b**) chord side.

4. SCFs at Key Hot Spot Locations on CHS-to-CFRHS Y-Joints

On the basis of the previous analysis of the influences of the significant non-dimensional geometric parameters on the SCF distribution, the maximum values of the SCFs of the CHS-to-CFRHS Y-joints subjected to axial tension in the brace are most likely to occur at the crown toe, 60° location or saddle. To determine empirical equations for SCFs at key hot spot locations (the crown toe, 60° location and saddle), it is necessary to investigate the influence of the significant non-dimensional geometric parameters (β, τ, γ and θ) on the SCFs at these locations of CHS-to-CFRHS Y-joints.

4.1. Influence of β on SCFs at Key Hot Spot Locations

The influences of β on SCFs at the crown toe, 60° location and saddle are illustrated in Figure 13. The SCF value initially increases, followed by a slight decrease at all the key hot spot locations (the crown toe, 60° location and saddle) on both the chord and the brace side. The peak SCF appears between β = 0.4 and 0.6 at all the key hot spot locations. Consequently, the width of the brace should be avoided to be set to half of the width of the chord to avoid high stress concentrations that lead to poor fatigue performance of CHS-to-CFRHS Y-joints.

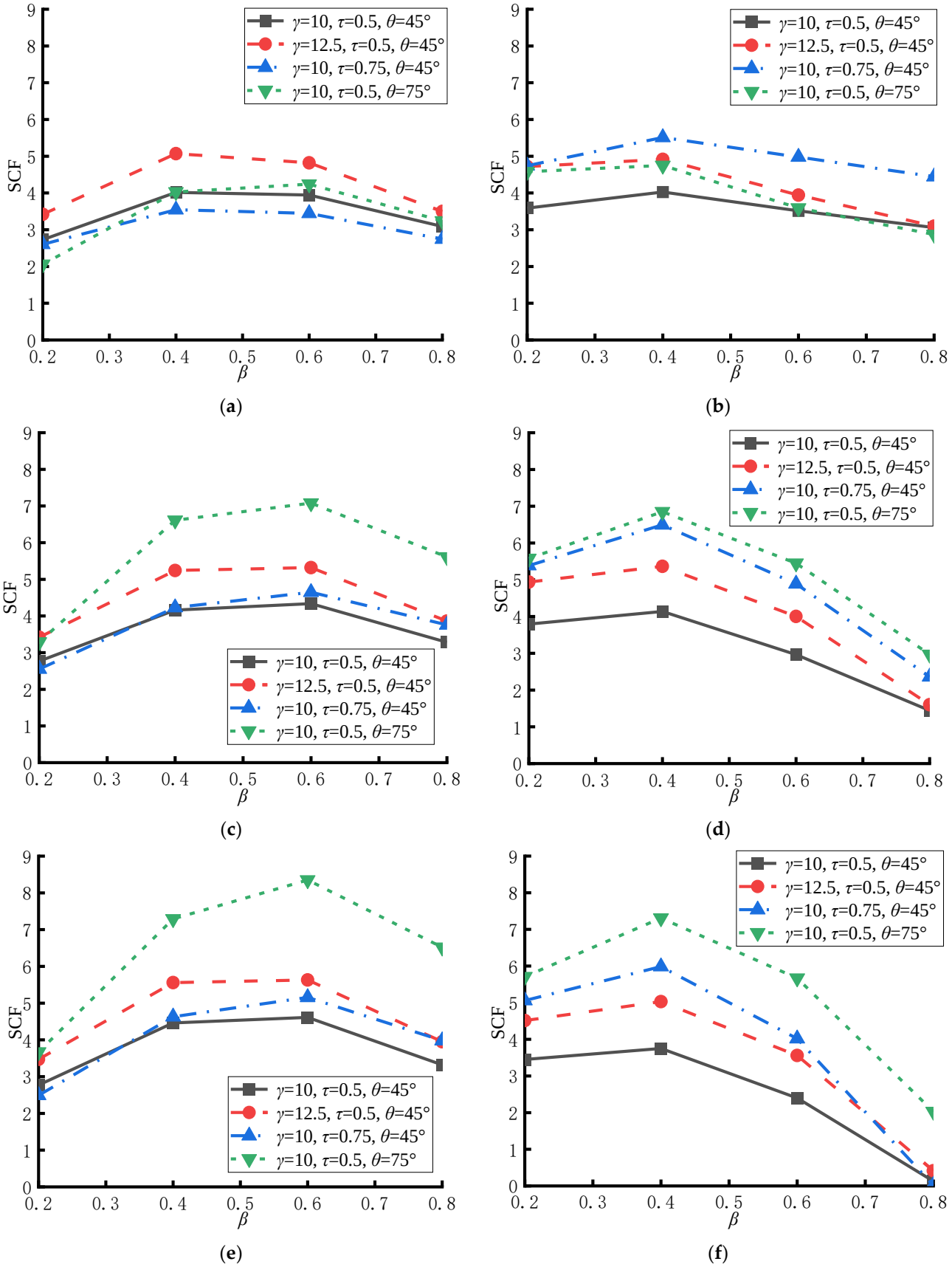


Figure 13. Influence of β on SCFs at key hot spot locations: (**a**) at the crown toe in the brace; (**b**) at the crown toe in the chord; (**c**) at the 60° location in the brace; (**d**) at the 60° location in the chord; (**e**) at the saddle in the brace; (**f**) at the saddle in the chord.

4.2. Influence of γ on SCFs at Key Hot Spot Locations

The influences of γ on SCFs at the crown toe, 60° location and saddle are illustrated in Figure 14. The values of the SCFs exhibit a constant linear increase at all the key hot spot locations on both the chord and the brace side. Therefore, increasing the thickness of the chord can reduce the stress concentrations and improve the fatigue performance of CHS-to-CFRHS Y-joints.

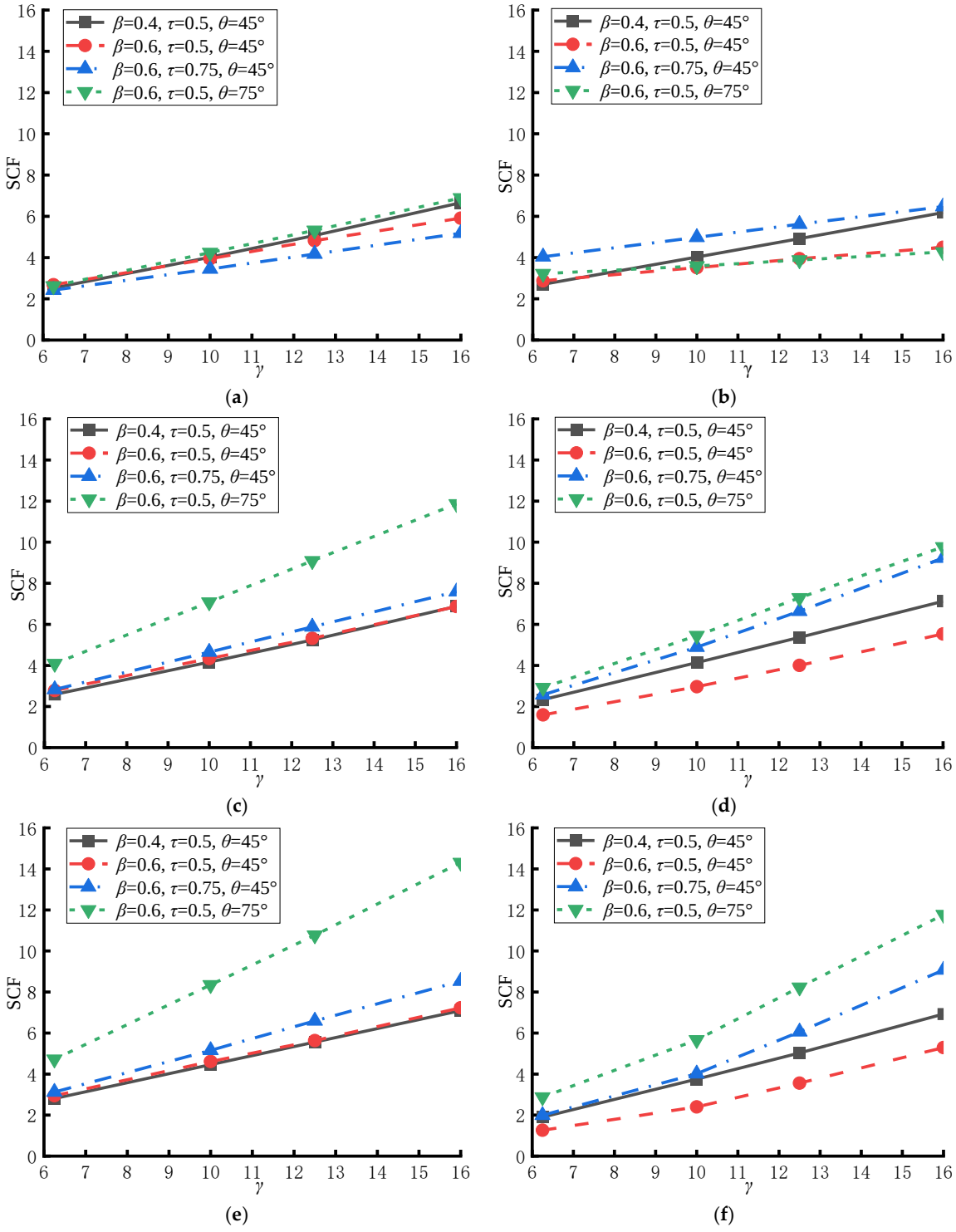


Figure 14. Influence of γ on SCFs at key hot spot locations: (**a**) at the crown toe in the brace; (**b**) at the crown toe in the chord; (**c**) at the 60° location in the brace; (**d**) at the 60° location in the chord; (**e**) at the saddle in the brace; (**f**) at the saddle in the chord.

4.3. Influence of τ on SCFs at Key Hot Spot Locations

The influences of τ on SCFs at the crown toe, 60° location and saddle are illustrated in Figure 15. The values of the SCFs on the chord side show a constant linear increase at all the key hot spot locations, whereas the values of the SCFs on the brace side initially increase and then slightly decrease at the crown toe.

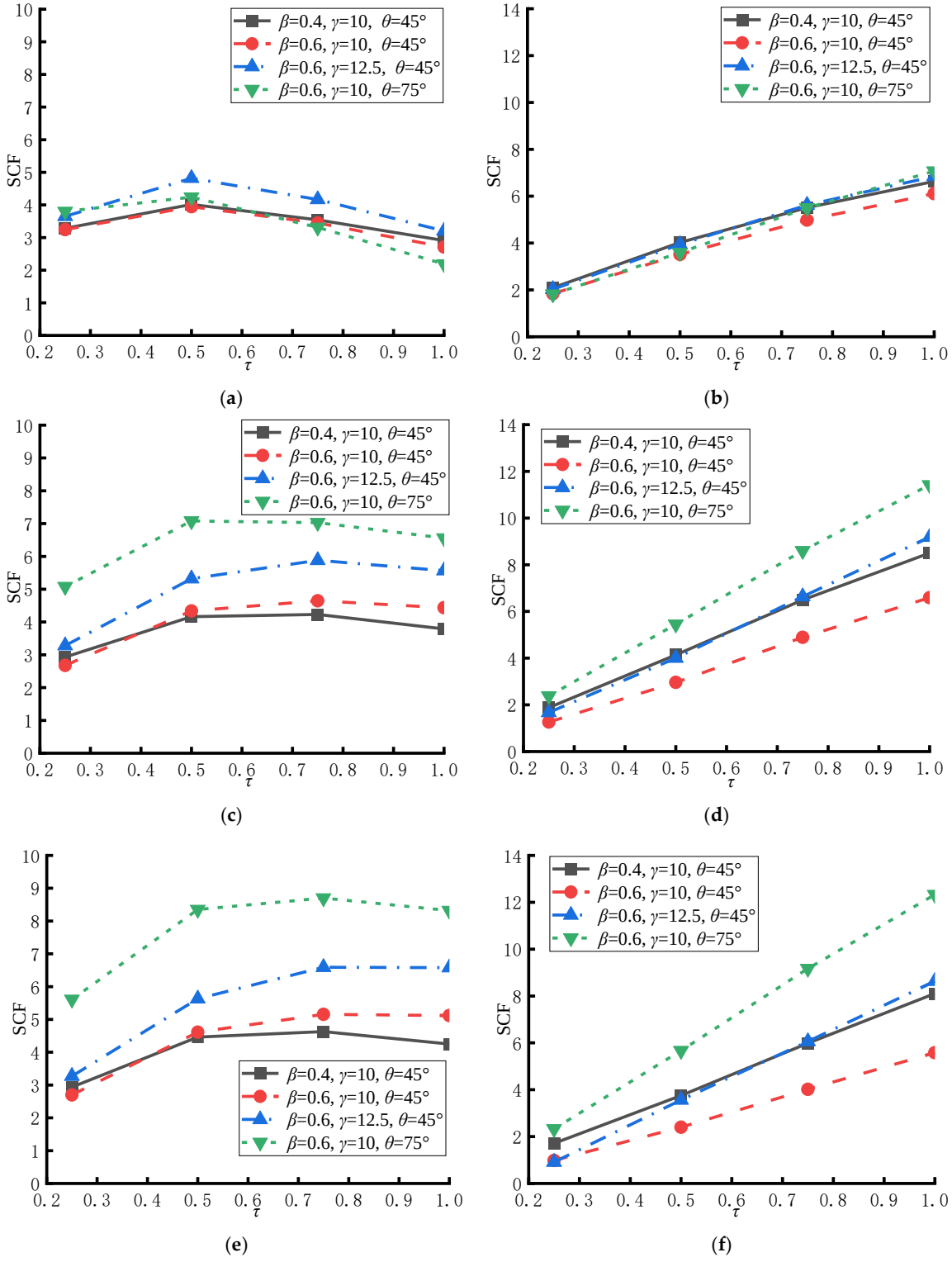


Figure 15. Influence of τ on SCFs at key hot spot locations: (**a**) at the crown toe in the brace; (**b**) at the crown toe in the chord; (**c**) at the 60° location in the brace; (**d**) at the 60° location in the chord; (**e**) at the saddle in the brace; (**f**) at the saddle in the chord.

4.4. Influence of θ on SCFs at Key Hot Spot Locations

The influences of θ on SCFs at the crown toe, 60° location and saddle are illustrated in Figure 16. The values of the SCFs at the 60° location and saddle increase as the value of θ increases, reaching the maximum values when the value of θ reaches 90°, on both the chord and the brace side. The results indicate that the value of θ has an important influence on the magnitude of the SCF values.

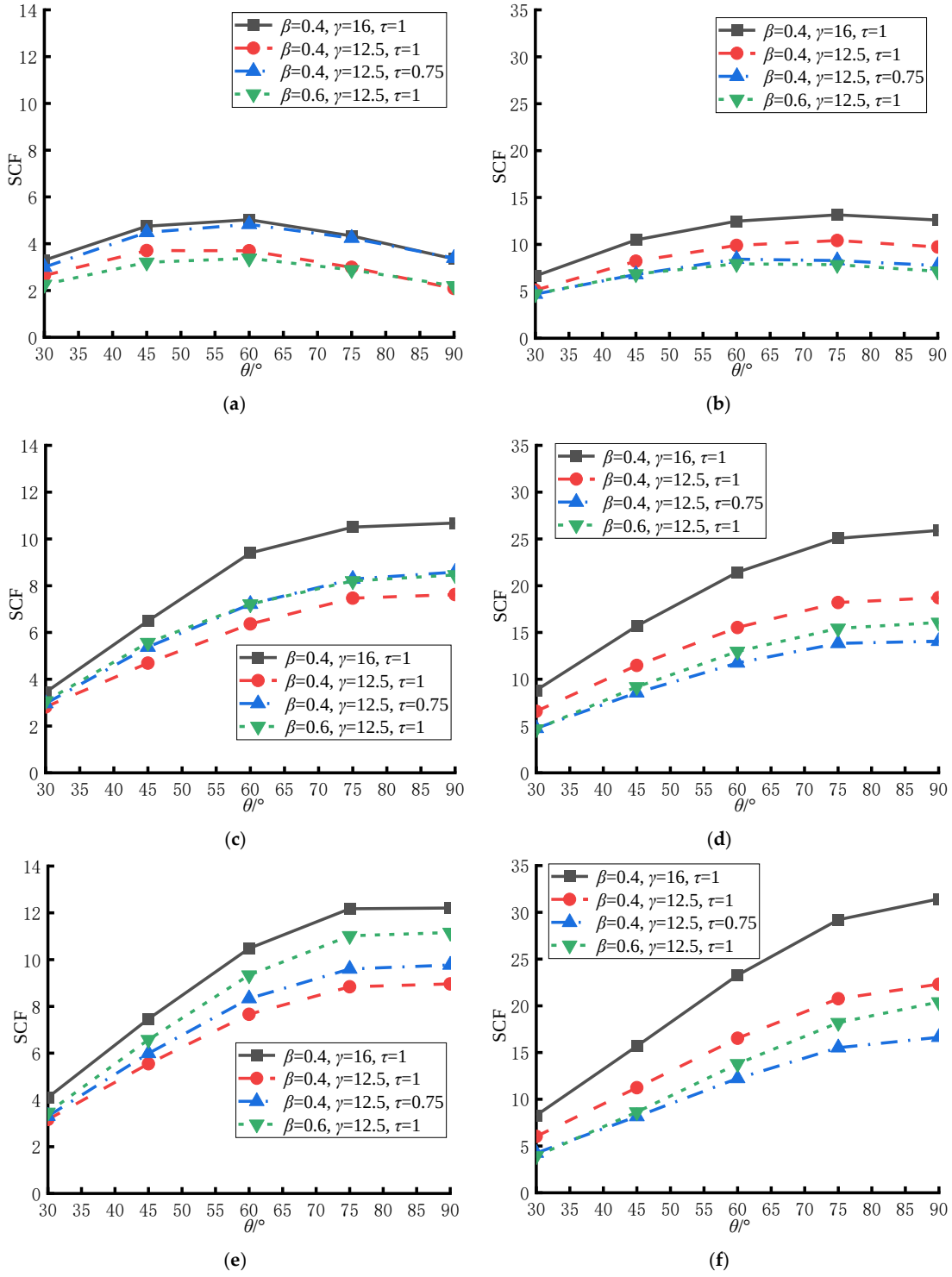


Figure 16. Influence of θ on SCFs at key hot spot locations: (**a**) at the crown toe in the brace; (**b**) at the crown toe in the chord; (**c**) at the 60° location in the brace; (**d**) at the 60° location in the chord; (**e**) at the saddle in the brace; (**f**) at the saddle in the chord.

5. Proposed Design Equations

5.1. Multiple Regression Analysis

On the basis of the correlation between the SCFs of CHS-to-CFRHS Y-joints at key hot spot locations (crown toe, 60° location and saddle) and the significant non-dimensional geometric parameters (β, τ, γ and θ), referring to the equations for RHS-to-RHS T-joints (CIDECT [46]), RHS-to-CFRHS T- and X-joints (Jiang et al. [23,24]), CHS-to-RHS T-joints (Tong et al. [50]), CHS-to-CFRHS T-joints (Tong et al. [39]) and RHS-to-CFRHS Y-joints (Jiang et al. [21]), Equation (3) was selected to obtain the empirical design equations to calculate the SCFs of CHS-to-CFRHS Y-joints via multiple regression analysis.

$$SCF = (c_1 + c_2 \cdot \beta + c_3 \cdot \beta^2) \cdot (2\gamma)^{c_4 + c_5 \cdot \beta + c_6 \cdot \beta^2} \cdot \tau^{c_7 + c_8 \cdot \beta} \cdot (\sin\theta)^{c_9} \quad (3)$$

where the values of c_1 to c_9 are determined via multiple regression analysis. The empirical design equations were obtained to calculate the SCFs of CHS-to-CFRHS Y-joints at the crown toe, 60° location and saddle, as shown in Equations (4)–(6) (brace side) and Equations (7)–(9) (chord side). The range of validity for CHS-to-CFRHS Y-joints in the empirical design equations is as follows: $0.2 \le \beta \le 0.8$, $6.25 \le \gamma \le 16$, $0.25 \le \tau \le 1.0$ and $30° \le \theta \le 90°$.

- At the crown toe in the brace:

$$SCF_{\text{brace, crown toe}} = (-0.00420 + 0.439\beta - 0.143\beta^2) \cdot (2\gamma)^{1.093 + 0.104\beta - 0.698\beta^2} \cdot \tau^{-0.0248 - 0.242\beta} \cdot (\sin\theta)^{0.376} \quad (4)$$

- At the 60° location in the brace:

$$SCF_{\text{brace, 60° location}} = (-0.00777 + 0.374\beta + 0.188\beta^2) \cdot (2\gamma)^{1.247 + 0.221\beta - 0.812\beta^2} \cdot \tau^{-0.0477 + 0.445\beta} \cdot (\sin\theta)^{1.423} \quad (5)$$

- At the saddle in the brace:

$$SCF_{\text{brace, saddle}} = (-0.0122 + 0.645\beta - 0.302\beta^2) \cdot (2\gamma)^{1.086 + 0.669\beta - 0.808\beta^2} \cdot \tau^{-0.101 + 0.733\beta} \cdot (\sin\theta)^{1.754} \quad (6)$$

- At the crown toe in the chord:

$$SCF_{\text{chord, crown toe}} = (0.232 - 2.007\beta + 7.770\beta^2) \cdot (2\gamma)^{1.857 - 2.905\beta + 0.984\beta^2} \cdot \tau^{0.775 + 0.241\beta} \cdot (\sin\theta)^{0.725} \quad (7)$$

- At the 60° location in the chord:

$$SCF_{\text{chord, 60° location}} = (-0.0517 + 1.232\beta - 1.236\beta^2) \cdot (2\gamma)^{1.537 - 0.595\beta + 0.343\beta^2} \cdot \tau^{0.851 + 0.504\beta} \cdot (\sin\theta)^{1.571} \quad (8)$$

- At the saddle in the chord:

$$SCF_{\text{chord, saddle}} = (0.141 + 0.150\beta - 0.319\beta^2) \cdot (2\gamma)^{1.256 + 1.078\beta - 0.869\beta^2} \cdot \tau^{0.876 + 0.543\beta} \cdot (\sin\theta)^{2.088} \quad (9)$$

5.2. Verification of the Design Equations

The ratio of the SCFs calculated via the empirical design equations ($SCF_{Equation}$) to the SCFs obtained via the FE models (SCF_{FE}) was used to validate the reliability of the empirical design equations, as shown in Figure 17. As shown in Table 3, the mean values of the $SCF_{Equation}$-to-SCF_{FE} ratios at key hot spot locations are between 0.97 and 1.01, and the COVs at key hot spot locations are less than 0.18. These results demonstrate the accuracy and reliability of the empirical design equations. In the fatigue design of engineering structures, the final design equations for SCF calculations at key hot spot locations (the crown toe, 60° location and saddle) in CHS-to-CFRHS Y-joints on both the chord and the

brace side should be modified by applying a safety factor of 1.2 [51] to ensure the safety of engineering structures, as shown in Equation (10). Additionally, the minimum value of the SCFs is specified to be no less than 2.0 to ensure that the results of the SCF calculations are conservative in the fatigue design of engineering structures [35].

$$SCF_{\text{Design}} = 1.2SCF_{\text{Equation (4) – (9)}} \quad (10)$$

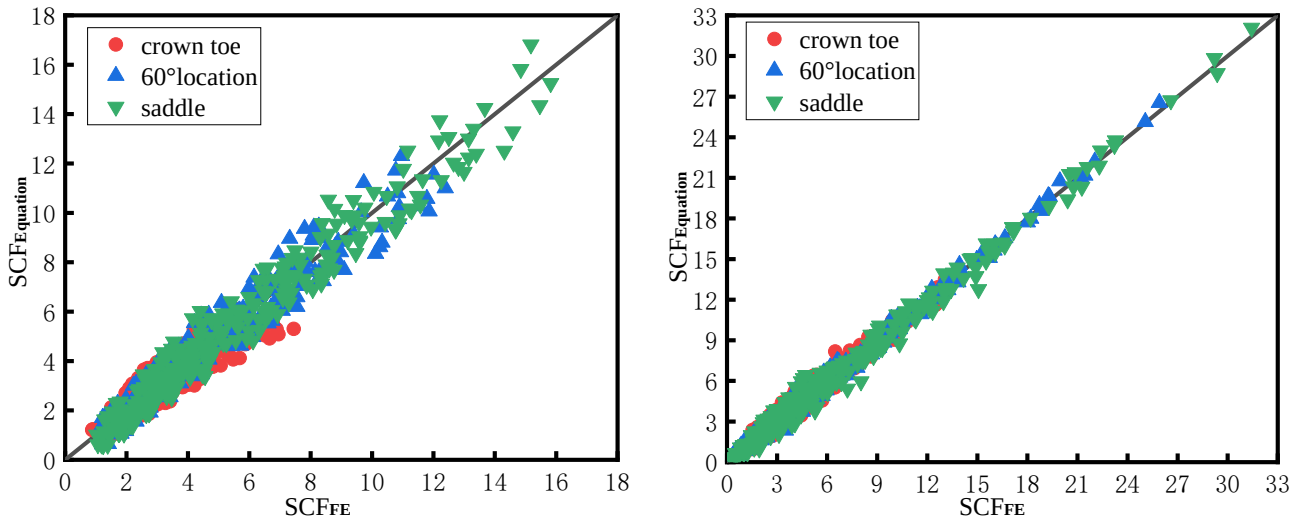


Figure 17. Comparison of the SCFs calculated via the empirical design equations and the SCFs obtained via the FE models: (**a**) brace side; (**b**) chord side.

Table 3. Comparative analysis of the SCFs calculated via the empirical design equations and the SCFs obtained via the FE models.

$SCF_{Equation}/SCF_{FE}$	At Crown Toe in Brace	At 60° Location in Brace	At Saddle in Brace	At Crown Toe in Chord	At 60° Location in Chord	At Saddle in Chord
Mean	0.97	0.98	0.97	1.00	1.01	0.99
COVs	0.18	0.16	0.16	0.13	0.12	0.14

6. Comparative Analysis of the SCFs for CHS-to-CFRHS Y-Joints and CHS-to-RHS Y-Joints

A modelling method similar to that utilised for CHS-to-CFRHS Y-joint is employed for CHS-to-RHS Y-joint, with the sole difference being that the FE model of CHS-to-RHS Y-joint does not require the simulation of concrete infilled into the chord. Eight FE models of the CHS-to-CFRHS Y-joints and the CHS-to-RHS Y-joints with the identical non-dimensional geometric parameters of $\beta = 0.4$, $\gamma = 10$, $\tau = 0.5$ and $\theta = 45°$; $\beta = 0.6$, $\gamma = 10$, $\tau = 0.5$ and $\theta = 45°$; $\beta = 0.4$, $\gamma = 10$, $\tau = 0.75$ and $\theta = 45°$; and $\beta = 0.4$, $\gamma = 10$, $\tau = 0.5$ and $\theta = 75°$ were established to determine the influence of infilling concrete on the SCFs along the weld profile for welded tubular Y-joints. The loading and boundary conditions of the FE models of the CHS-to-RHS Y-joints were the same as those of the FE models of the CHS-to-CFRHS Y-joints.

The comparison results of the SCFs along the weld profile between the CHS-to-RHS Y-joints and the CHS-to-CFRHS Y-joints are shown in Figure 18. The CHS-to-CFRHS Y-joints and CHS-to-RHS Y-joints exhibit the identical trends in the SCF distribution along the weld profile on both the chord and the brace side. Most of the cases exhibit a similar

trend: the SCF value generally has an initial increase followed by a slight decrease for CHS-to-CFRHS Y-joints and CHS-to-RHS Y-joints. Infilling concrete in the chord leads to a reduction in SCFs at all locations along the weld profile, and the reduction in SCFs along the weld profile is more than 15% in the chord and 11% in the brace on average. The peak SCF of the welded tubular Y-joint is decreased by more than 15.6% on the chord side and 15.2% on the brace side by infilling concrete in the chord. As shown in Figure 19, the sample deformation results of the welded tubular Y-joints under axial tension loading of the brace with parameters of β = 0.4, γ = 10, τ = 0.75 and θ = 45° indicate that the maximum deformation at the chord top wall of the welded tubular Y-joint is decreased by 29.5% by infilling concrete in the chord. For the CHS-to-RHS Y-joints subjected to axial tension loading of the brace, the chord side walls exhibit inwards deformation, and the chord top wall exhibits outwards deformation. Infilling concrete in the chord can limit the inwards deformation of the chord side walls and decrease the outwards deformation of the chord top wall, leading to lower bending stresses in the chord top wall which cause lower HSS and reduce the stress concentrations. In conclusion, infilling concrete in the chord for welded tubular joints can decrease the SCFs along the weld profile and peak SCF and reduce the deformation of the chord walls.

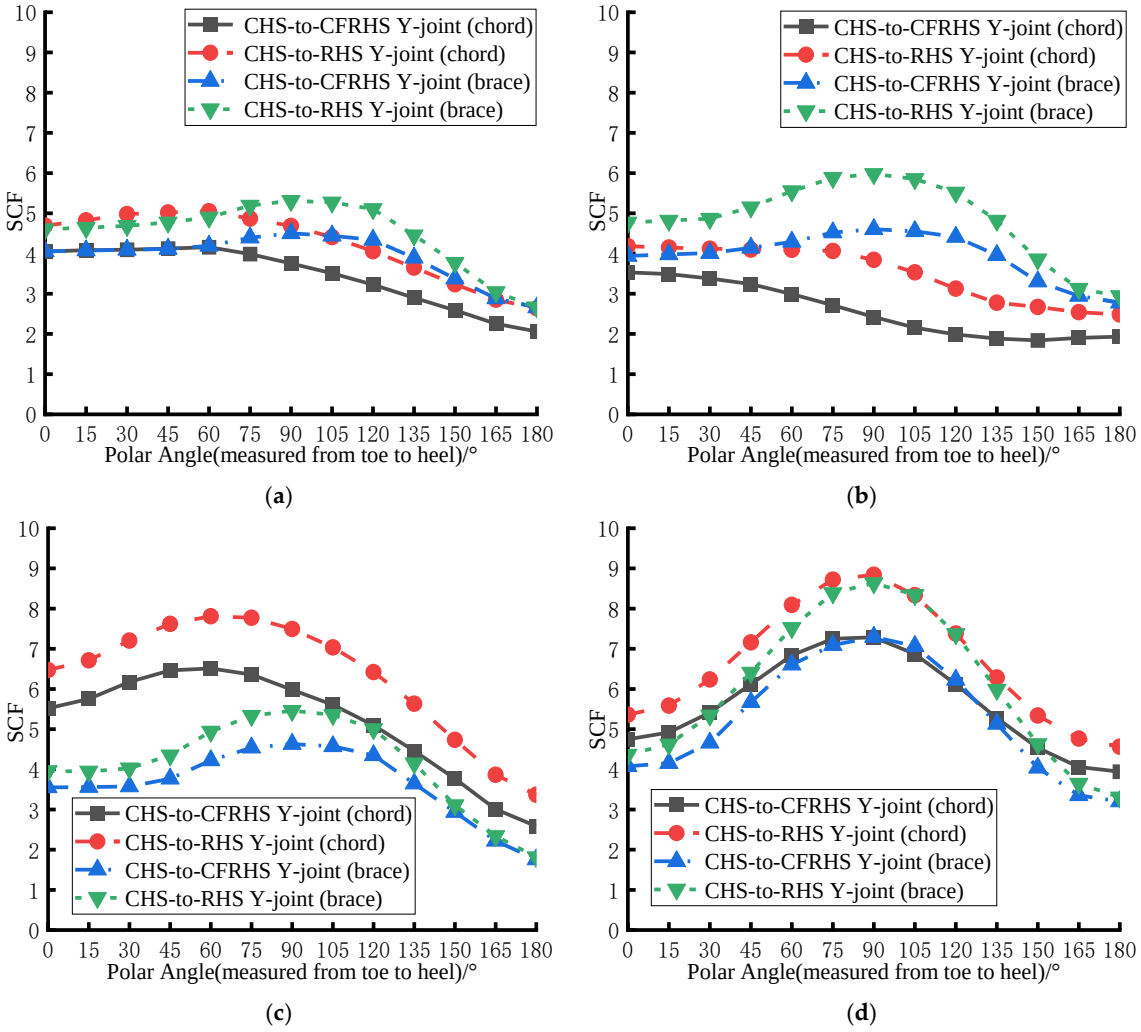
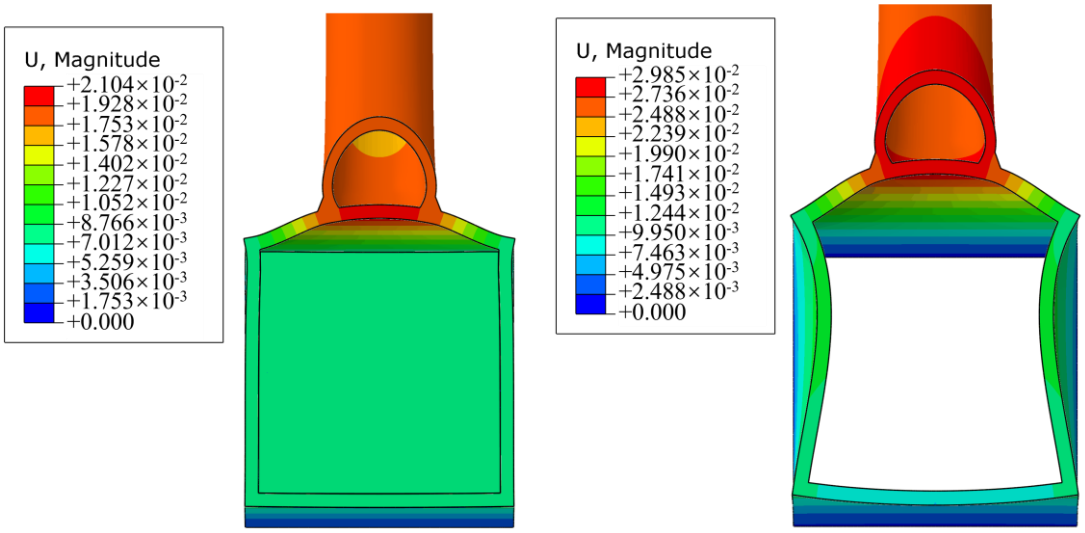


Figure 18. Influence of infilling concrete on the SCF distribution: (**a**) Y-joints with parameters β = 0.4, γ = 10, τ = 0.5, and θ = 45°; (**b**) Y-joints with parameters β = 0.6, γ = 10, τ = 0.5, and θ = 45°; (**c**) Y-joints with parameters β = 0.4, γ = 10, τ = 0.75, and θ = 45°; (**d**) Y-joints with parameters β = 0.4, γ = 10, τ = 0.5, and θ = 75°.



(**a**) (**b**)

Figure 19. Sample FE results of deformations for Y-joints under unit axial tension loading in the brace with parameters β = 0.4, γ = 10, τ = 0.75 and θ = 45°: (**a**) CHS-to-CFRHS Y-joint; (**b**) CHS-to-RHS Y-joint.

7. Conclusions

In this work, the stress concentrations of CHS-to-CFRHS Y-joints subjected to axial tension loading of the brace were investigated. A comprehensive parametric analysis was carried out to determine the effects of the non-dimensional geometric parameters on the SCFs of CHS-to-CFRHS Y-joints. Then, on the basis of the large database of the SCF results obtained from the FE models of the CHS-to-CFRHS Y-joints, a multiple regression analysis method was utilised to derive the empirical design equations for SCF calculations at the crown toe, 60° location and saddle of CHS-to-CFRHS Y-joints. Ultimately, a comparative analysis of the SCFs between the CHS-to-CFRHS Y-joints and the CHS-to-RHS Y-joints was conducted to determine the effects of infilling concrete in the chord on the SCFs of welded tubular joints. The main conclusions of this research can be drawn as follows:

1. When the CHS-to-CFRHS Y-joint is subjected to axial tension loading of the brace, on the chord side, the SCF values reach the maximum values at the crown toe, 60° location or saddle in most cases. On the brace side, the majority of the maximum SCF values are located at the saddle, with a minority at the crown toe.
2. For the CHS-to-CFRHS Y-joint under axial tension loading of the brace, as the value of β increases, the values of the SCFs initially increase and then decrease, reaching the maximum values between β = 0.4 and 0.6. Therefore, the width of the brace of the CHS-to-CFRHS Y-joint should not be set to half of the width of the chord to avoid high stress concentrations that lead to poor fatigue performance. As the value of γ increases, the values of the SCFs exhibit a constant linear increase. As a result, increasing the thickness of the chord of the CHS-to-CFRHS Y-joint can reduce stress concentrations and improve the fatigue performance.
3. The intersection angle of brace and chord has an important influence on the magnitudes of the SCF values on both the chord and the brace side of CHS-to-CFRHS Y-joints under axial tension loading of the brace. The values of the SCFs at the 60° location and saddle increase as the value of θ increases, reaching the maximum values when the value of θ reaches 90°, on both the chord and the brace side.
4. The empirical design equations proposed in this research for SCF calculations at the crown toe, 60° location and saddle of CHS-to-CFRHS Y-joints under axial tension

loading of the brace provide safe and reliable results. The SCFs calculated via the empirical design equations can be utilised to calculate the HSS and predict the fatigue life via the HSS method for the fatigue design of CHS-to-CFRHS Y-joints in a composite truss structure.

5. Infilling concrete in the chord for welded tubular joints can decrease the SCFs along the weld profile and peak SCF. In the comparison of the SCFs along the weld profile and peak SCF between the CHS-to-CFRHS Y-joints and the CHS-to-RHS Y-joints, infilling concrete in the chord leads to a reduction in SCFs along the weld profile of more than 15% in the chord and 11% in the brace on average, and the peak SCF is decreased by more than 15.6% on the chord side and 15.2% on the brace side.
6. For the CHS-to-CFRHS Y-joint under axial tension loading of the brace, the infilled concrete can limit the inwards deformation of the chord side walls and decrease the outwards deformation of the chord top wall, leading to lower HSS and reducing the stress concentrations.

Author Contributions: Conceptualisation, Y.F. and K.D.; methodology, Y.F.; software, Y.F. and K.D.; validation, Y.F. and K.D.; formal analysis, Y.F.; investigation, Y.F.; resources, Y.F.; data curation, Y.F.; writing—original draft preparation, Y.F.; writing—review and editing, Y.F.; visualisation, Y.F.; supervision, Y.F. and K.D.; project administration, Y.F. and K.D. All authors have read and agreed to the published version of the manuscript.

Funding: This research received no external funding.

Data Availability Statement: Data are contained within the article.

Conflicts of Interest: The authors declare no conflicts of interest.

References

1. Xiao, L.; Wei, X.; Zhao, J.M.; Wu, C.T. Hot spot stress concentration factor of CFST T/Y joints based on modified equivalent thickness. *Structures* **2023**, *51*, 910–925. [CrossRef]
2. Xu, F.; Chen, J.; Guo, Y.; Ye, Y. Innovative design of the world's tallest electrical transmission towers. *Proc. Inst. Civ. Eng.-Civ. Eng.* **2019**, *172*, 9–16. [CrossRef]
3. Packer, J.A. Concrete-filled HSS connections. *J. Struct. Eng.* **1995**, *121*, 458–467. [CrossRef]
4. Sakai, Y.; Hosaka, T.; Isoe, A.; Ichikawa, A.; Mitsuki, K. Experiments on concrete filled and reinforced tubular K-joints of truss girder. *J. Constr. Steel Res.* **2004**, *60*, 683–699. [CrossRef]
5. Han, L.H.; Li, W.; Bjorhovde, R. Developments and advanced applications of concrete-filled steel tubular (CFST) structures: Members. *J. Constr. Steel Res.* **2014**, *100*, 211–228. [CrossRef]
6. *EN 1993-1-8, 2005*; Eurocode 3: Design of Steel Structures, Part 1-8: Design of Joints. CEN: Brussels, Belgium, 2005.
7. *CIDECT Design Guide No.3*; Design Guide for Rectangular Hollow Section (RHS) Joints Under Predominantly Static Loading. Verlag TÜV Rheinland Gmb: Geneva, Switzerland, 2009.
8. Xu, F.; Chen, J.; Jin, W.L. Punching shear failure of concrete-filled steel tubular CHS connections. *J. Constr. Steel Res.* **2016**, *124*, 113–121. [CrossRef]
9. Xu, F.; Chen, J.; Jin, W.L. Experimental investigation and design of concrete-filled steel tubular CHS connections. *J. Struct. Eng.* **2015**, *141*, 04014106. [CrossRef]
10. Huang, W.J.; Fenu, L.; Chen, B.C.; Briseghella, B. Experimental study on K-joints of concrete-filled steel tubular truss structures. *J. Constr. Steel Res.* **2015**, *107*, 182–193. [CrossRef]
11. Xu, F.; Chen, J.; Chan, T.M. Mechanical behaviour of concrete-filled CHS connections subjected to in-plane bending. *Eng. Struct.* **2017**, *148*, 101–112. [CrossRef]
12. Song, S.S.; Chen, J.; Xu, F. Mechanical behaviour and design of concrete-filled K and KK CHS connections. *J. Constr. Steel Res.* **2022**, *188*, 107000. [CrossRef]
13. Hou, C.; Han, L.H.; Zhao, X.L. Concrete-filled circular steel tubes subjected to local bearing force: Experiments. *J. Constr. Steel Res.* **2013**, *83*, 90–104. [CrossRef]
14. Hou, C.; Han, L.H.; Zhao, X.L. Concrete-filled circular steel tubes subjected to local bearing force: Finite element analysis. *Thin-Walled Struct.* **2014**, *77*, 109–119. [CrossRef]

15. Yang, Y.F.; Hou, C.; Wen, Z.; Han, L.H. Experimental behaviour of square CFST under local bearing forces. *Thin-Walled Struct.* **2014**, *74*, 166–183. [CrossRef]
16. Ma, Y.P.; Liu, Y.J.; Wang, K.; Liu, J.; Zhang, Z.J. Axial stiffness of concrete filled rectangular steel tubular (CFRST) truss joints. *J. Constr. Steel Res.* **2021**, *184*, 106820. [CrossRef]
17. Xu, F.; Chen, J.; Jin, W.L. Experimental investigation of SCF distribution for thin-walled concrete-filled CHS joints under axial tension loading. *Thin-Walled Struct.* **2015**, *93*, 149–157. [CrossRef]
18. Jiang, L.; Liu, Y.J.; Fam, A. Stress concentration factors in concrete-filled square hollow section joints with perfobond ribs. *Eng. Struct.* **2019**, *181*, 165–180. [CrossRef]
19. Jiang, L.; Liu, Y.J.; Fam, A.; Wang, K.N. Fatigue behaviour of non-integral Y-joint of concrete-filled rectangular hollow section continuous chord stiffened with perfobond ribs. *Eng. Struct.* **2019**, *191*, 611–624. [CrossRef]
20. Jiang, L.; Liu, Y.J.; Fam, A.; Liu, J.; Liu, B. Stress concentration factor parametric formulae for concrete-filled rectangular hollow section K-joints with perfobond ribs. *J. Constr. Steel Res.* **2019**, *160*, 579–597. [CrossRef]
21. Jiang, L.; Liu, Y.J.; Liu, J.; Liu, B. Experimental and numerical analysis of the stress concentration factor for concrete-filled square hollow section Y-joints. *Adv. Struct. Eng.* **2020**, *23*, 869–883. [CrossRef]
22. Tong, L.W.; Xu, G.; Yan, D.; Zhao, X. Fatigue tests and design of diamond bird beak SHS T-joints under axial loading in brace. *J. Constr. Steel Res.* **2016**, *118*, 49–59. [CrossRef]
23. Jiang, L.; Liu, Y.J.; Amir, F. Stress concentration factors in joints of square hollow section (SHS) brace and concrete-filled SHS chord under axial tension in brace. *Thin-Walled Struct.* **2018**, *132*, 79–92. [CrossRef]
24. Gao, L.; Jiang, L.; Wang, X.; Gao, S.; Cui, H.; Liu, J.; Zhou, H. Expressions for Stress Concentration Factors for T-Joints of Hollow and Concrete-Filled Square Cross-Sections for In-Plane Axial and Bending Loads. *Symmetry* **2024**, *16*, 1082. [CrossRef]
25. Matti, F.; Mashiri, F. Stress Concentration Factors of Concrete-Filled T-Joints under In-Plane Bending: Experiments, FE Analysis and Formulae. *Materials* **2022**, *15*, 6421. [CrossRef] [PubMed]
26. Matti, F.; Mashiri, F. Design formulae for predicting the stress concentration factors of concrete-filled T-joints under out-of-plane bending. *Structures* **2020**, *28*, 2073–2095. [CrossRef]
27. Musa, I.; Mashiri, F.; Zhu, X.Q. Parametric study and equation of the maximum SCF for concrete filled steel tubular T-joints under axial tension. *Thin-Walled Struct.* **2018**, *129*, 145–156. [CrossRef]
28. Musa, I.; Mashiri, F. Parametric study and equations of the maximum SCF for concrete filled steel tubular T-joints under in-plane and out-of-plane bending. *Thin-Walled Struct.* **2019**, *135*, 245–268. [CrossRef]
29. Musa, I.; Mashiri, F.; Zhu, X.Q.; Tong, L.W. Experimental stress concentration factor in concrete-filled steel tubular T-joints. *J. Constr. Steel Res.* **2018**, *150*, 442–451. [CrossRef]
30. Chen, J.; Chen, J.; Jin, W.L. Experiment investigation of stress concentration factor of concrete-filled tubular T joints. *J. Constr. Steel Res.* **2010**, *66*, 1510–1515. [CrossRef]
31. Zheng, J.; Nakamura, S.; Ge, Y.J.; Chen, K.M.; Wu, Q. Formulation of stress concentration factors for concrete-filled steel tubular (CFST) T-joints under axial force in the brace. *Eng. Struct.* **2018**, *170*, 103–117. [CrossRef]
32. Zhao, J.M.; Xiao, L.; Wei, X.; Li, X. Parametric study and neural network-based prediction for stress concentration factor of concrete-filled steel tubular T-joint. *Ocean. Eng.* **2024**, *305*, 117972. [CrossRef]
33. Mashiri, F.; Zhao, X.; Tong, L.W. Fatigue tests and design of thin CHS-SHS Tjoints under cyclic in-plane bending. *J. Civ. Struct. Health Monit.* **2013**, *3*, 129–140. [CrossRef]
34. Packer, J.; Mashiri, F.; Zhao, X.; Willibald, S. Static and fatigue design of CHS-to-RHS welded connections using a branch conversion method. *J. Constr. Steel Res.* **2007**, *63*, 82–95. [CrossRef]
35. Yin, Y.; Liu, X.; Lei, P.; Zhou, L. Stress concentration factor for tubular CHS-to-RHS Y-joints under axial loads. *J. Constr. Steel Res.* **2018**, *148*, 768–778. [CrossRef]
36. Tong, L.W.; Xu, G.W.; Yang, D.L.; Mashiri, F.; Zhao, X.L. Fatigue behavior and design of welded tubular T-joints with CHS brace and concrete-filled chord. *Thin-Walled Struct.* **2017**, *120*, 180–190. [CrossRef]
37. Tong, L.W.; Yang, D.L.; Zhao, X.L. Tests for fatigue behavior of welded CHS-SHS-concrete filled T-joints. *J. Vib. Shock* **2013**, *32*, 99–105.
38. Yang, D.L.; Tong, L.W. Calculation formula of SCF for CHS-CFSHS welded T-joints with brace under axial tension. *J. Jilin Univ. (Eng. Technol. Ed.)* **2019**, *49*, 1891–1899.
39. Tong, L.W.; Xu, G.W.; Yang, D.L.; Mashiri, F.; Zhao, X.L. Stress concentration factors in CHS-CFSHS T-joints: Experiments, FE analysis and formulae. *Eng. Struct.* **2017**, *151*, 406–421. [CrossRef]
40. Morgan, M.; Lee, M. Prediction of stress concentrations and degrees of bending in axially loaded tubular K-joints. *J. Constr. Steel Res.* **1998**, *45*, 67–97. [CrossRef]
41. *GB50017-2017*; Chinese Standard: Standard for Design of Steel Structures. Ministry of Housing and Urban-Rural Development of the People's Republic of China: Beijing, China, 2017.

42. *GB50010-2010*; Chinese Standard: Code for Design of Concrete Structures. Ministry of Housing and Urban-Rural Development of the People's Republic of China: Beijing, China, 2010.
43. *ANSI/AWS D1.1-96*; Structural Welding Code-Steel. American Welding Society, Inc.: Miami, FL, USA, 1996.
44. Wang, K. Stress Concentration Factors and Fatigue Behavior of Welded T-Joints with a CHS Brace and a CFCHS Chord. Ph.D. Thesis, Tongji University, Shanghai, China, 2008.
45. *IIW Doc. No. XV-582-85*; Recommended Fatigue Design Procedure for Welded Hollow Section Joints, Part 1-Hot Spot Stress Method for Nodal Joints. IIW Subcommission XV-E: Strasburg, France, 1985.
46. *CIDECT Design Guide No.8*; Design Guide for Circular and Rectangular Hollow Section Welded Joints Under Fatigue Loading. TÜV-Verlag: Cologne, Germany, 2000.
47. American Petroleum Institute. *Planning, Designing and Constructing Fixed Offshore Platforms—Working Stress Design*, 22nd ed.; API RP 2A-WSD (R2020); American Petroleum Institute: Washington, DC, USA, 2014.
48. DNVGL. *Fatigue Design of Offshore Steel Structures*; DNVGL-RP-C203; DNVGL: Oslo, Norway, 2016.
49. Zhao, R.; Liu, Y.J.; Jiang, L.; Fu, Y.S.; Zhao, Y.D.; Zhao, X.D. Degree of bending of concrete-filled rectangular hollow section K-joints under balanced-axial loadings. *Front. Struct. Civ. Eng.* **2022**, *16*, 461–477. [CrossRef]
50. Tong, L.W.; Zheng, H.; Mashiri, F.; Zhao, X. Stress-concentration factors in circular hollow section and square hollow section T-connections: Experiments, finite-element analysis, and formulas. *J. Struct. Eng.* **2013**, *139*, 1866–1881. [CrossRef]
51. Liu, Y.J.; Zhao, R.; Jiang, L.; Fu, Y.S. Study on Calculation Method for Equivalent Stress Intensity Factor of Rectangular Hollow Section K-Joints. *Eng. Mech.* **2023**, *40*, 182–194.

Disclaimer/Publisher's Note: The statements, opinions and data contained in all publications are solely those of the individual author(s) and contributor(s) and not of MDPI and/or the editor(s). MDPI and/or the editor(s) disclaim responsibility for any injury to people or property resulting from any ideas, methods, instructions or products referred to in the content.